JOHN C. MURPHY, JANE W. MACLACHLAN, and LEONARD C. AAMODT

THERMAL TECHNIQUES FOR NONDESTRUCTIVE CHARACTERIZATION OF LAYERED STRUCTURES AND INTERFACES

Many recent technological advances are based on the development of new materials engineered to have enhanced properties. Certain desirable properties that result are acquired by combining distinct materials that have markedly different physical properties. The structural aspects of these new materials and the extended property ranges they exhibit have introduced the need for improved methods of characterization, both during the fabrication process and during use. In this article we review some recent developments in thermal methods for characterizing layered structures and describe some specific applications of the methods.

INTRODUCTION

Thermal nondestructive evaluation techniques are well suited for characterizing the surface and subsurface properties of multicomponent, layered systems of materials, particularly when the components of the systems have different thermal properties.[1-3] Examples of these systems are protective coatings on sensitive substrates, composite materials, and multilayered integrated circuits. As an example of what thermal techniques for nondestructive characterization can reveal, consider ceramic coatings on metallic substrates. Analysis of the thermal response can reveal variations in coating thickness, coating thermal properties, substrate thermal properties, and the nature of the bond between the coating and the substrate. Composite materials, including metal matrix systems in which there are particles or fibers of low thermal conductivity in a matrix of high thermal conductivity, are another important area for applying thermal nondestructive evaluation techniques. For integrated-circuit multilayers, the issues surrounding buried-layer thermal and electronic properties and the characteristics of interfaces between layers are critical for many applications.

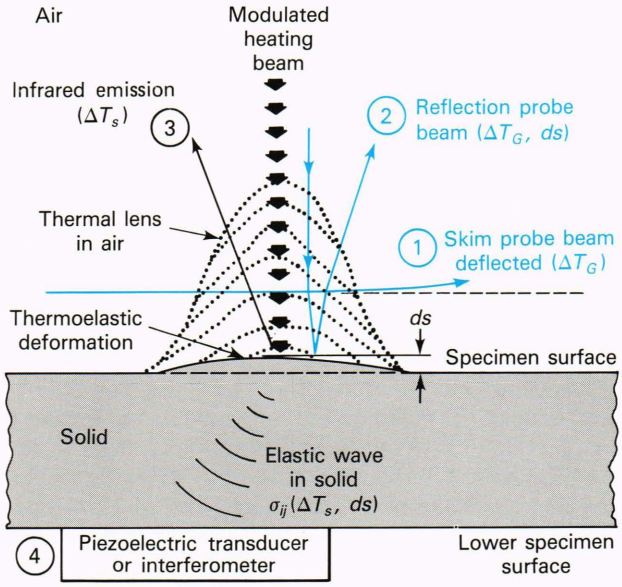

Figure 1—Physical processes occurring during a thermal-wave measurement, indicating the available range of detection techniques: (1) optical-beam deflection, (2) reflective optical-beam deflection, (3) infrared radiometry, and (4) thermoelastic (transducer or interferometric) detection. (T_G is the gas temperature.)

FUNDAMENTALS OF THERMAL-WAVE IMAGING

The basic processes of thermal measurements for materials characterization are summarized in Fig. 1, which shows a modulated pump (heating) beam striking a specimen surface and producing a change in specimen temperature, ΔT_s. Laser, electron, ion, and X-ray beams can all be used as the pump beam; the changes in the energy-deposition profile and the subsequent temperature distribution in the material depend on what source is selected for the beam. Tailoring the energy deposition in the specimen by the appropriate selection of beam wavelength or energy can significantly affect the contrast observed in detecting subsurface features (see, for example, Fig. 5 in Ref. 1). A key factor in time-resolved thermal imaging techniques is that the heating source is modulated in time to create in the material a dynamic temperature response rather than a steady-state response. The modulation can either be continuous wave at one particular modulation frequency (i.e., thermal-wave imaging) or pulsed, using pulses of a particular duration.

A dynamic temperature field is set up in the sample by the heating process; the spatial extent, magnitude, and phase of this temperature field depend on the initial heat-deposition profile in the specimen, on the thermal prop-

erties of the specimen, and on the conversion or transport of energy in the specimen. An example of energy conversion is the elastic disturbance created in the specimen as a result of thermoelastic expansion. The coupled thermoelastic equations that give the temperature and elastic displacements in the specimen are

$$\nabla^2 T - \alpha^{-1}\,\partial T/\partial t = -H/k + (T\beta_t B/k)\nabla \cdot \partial \mathbf{u}/\partial t \tag{1}$$

and

$$\nabla^2 \mathbf{u} + (1 + \lambda/\mu)\nabla(\nabla \cdot \mathbf{u}) - (\rho/\mu)\partial^2 \mathbf{u}/\partial t^2 = (\beta_t B/\mu)\nabla T\ , \tag{2}$$

where T is the temperature, $\mathbf{u}$ is the elastic displacement vector, k is the thermal conductivity, α is the thermal diffusivity, β_t is the volume thermal expansion coefficient, λ and μ are the Lamé constants, ρ is the density, B is the bulk modulus, and H is the thermal source term.

Equation 1 is the thermal diffusion equation with the addition of the second heating term (on the right), originating from the particle displacements associated with an elastic wave. This additional term is usually neglected, and Eq. 1 is used to calculate the temperature distribution in the specimen. This temperature solution is used as a source term in Eq. 2, which is the thermoelastic equation.

The main consequences of Eqs. 1 and 2 are that, for spatially uniform heating, the temperature in the specimen decreases exponentially with depth, z, as $\exp(-z/\delta)$, where

$$\delta = (\alpha/\pi f)^{1/2} \tag{3}$$

is the thermal diffusion length and f is the modulation frequency of the pump beam. For a modulation frequency of 1 Hz, δ is about 3 mm in a typical metal while for a ceramic, δ is about 0.2 mm. At 1 MHz, the values for δ in a metal and a ceramic decrease to 3 μm and 0.2 μm, respectively. For nonuniform heating, the analytical results are similar but are modified to reflect the distribution of spatial frequencies determined by the spatial extent of the source and the loss of spatial detail associated with the diffusion process. Hence, the lateral spatial resolution possible with thermal-wave-imaging techniques depends on a variety of factors including the thermal properties of the medium, the modulation frequency of the pump beam, and the size of the pump beam. For near-surface features, the size of the pump beam is the most important factor in determining the lateral resolution. For deeper features, the thermal properties play a larger role, leading to the conclusion that for successfully imaging subsurface features, the size of the pump beam and the depth of the feature should be roughly equal for best spatial resolution.

Several experimental methods used for monitoring the temperature distribution are shown (labeled 1, 2, 3, and 4) in Fig. 1. Complete details of these methods can be found in Ref. 1 and in the references therein, but note that there is a wide range of physical phenomena used for detection. The optical-beam-deflection techniques (methods 1 and 2) rely on the formation of a thermal lens resulting from variations in the index of refraction of air when heat is conducted from the specimen to the air layer above it. The deflection of a probing laser beam sent through this lens is proportional to the specimen temperature. Infrared detection (method 3) is used to monitor specimen temperature by measuring the enhanced infrared emission from the specimen. Thermoelastic techniques (method 4) detect the specimen's elastic response resulting from thermoelastic expansion in the heated region.

These techniques are indirect measures of temperature distribution in the specimen, and the responses must be calibrated in order to be measures of absolute temperature. Some detection methods, however, are better suited than others for specific specimen geometries and combinations of material properties. In the following sections three thermal nondestructive evaluation techniques for characterizing layered structures are discussed in detail: (1) time-resolved infrared techniques, (2) thermoelastic techniques, and (3) internal optical-beam-deflection probing techniques. Examples of the application of these techniques for evaluating the ceramic thermal-barrier coatings on metal superalloys used in jet engines and for measuring the thermal and electronic transport in semiconductors are also given.

TIME-RESOLVED INFRARED TECHNIQUES

Several thermal-wave inspection techniques for coating systems have been developed, including thermal-wave interferometry,[4] pulsed photothermal radiometry,[5] and time-resolved infrared techniques.[6] The time-resolved infrared technique involves monitoring changes in specimen surface temperature that are indications of the dynamic heat flow in the material in response to application of a transient heating source. These techniques are in contrast to the more conventional industrial thermographic techniques where steady-state temperatures are monitored. The extension from steady-state to time-resolved infrared techniques has been gaining popularity rapidly; in its most frequently practiced form, a single pulse of heat energy is applied to a specimen, usually by a laser, and the time decay of the surface temperature is monitored. This short-pulse technique is generally termed flash radiometry or pulsed photothermal radiometry[7]; it has been used to measure thermal diffusivities in many materials from polymer films[8] to bruises[9] and to study the bonding of coatings.[10]

In our work we have been using a step heating source and monitoring the specimen surface temperature as a function of time while heat is applied to the specimen. The heating pulse is turned off after a set time, τ, and the surface temperature is monitored while the specimen cools. Step heating allows the heating flux to be at a much lower value than that needed for pulse heating because the heat is applied over a longer time. Hence, for specimens with long thermal diffusion times, the peak specimen temperatures experienced during the measure-

ment are lower than in the pulse case, and the possibility of thermal damage to the specimen is consequently reduced. In addition, with step heating both the heating and cooling time regimes are accessible and provide additional information about the thermal and structural characteristics of the specimen.

The time-resolved infrared technique was developed because there were difficulties when conventional continuous-wave modulated thermal-wave methods were used to study thick specimens having low thermal diffusivity. From the typical values for the thermal diffusivities of metals and ceramics given above, it is clear that for a 200-mm-thick ceramic coating, a modulation frequency of less than 1 Hz is required to provide a thermal-diffusion length great enough to extend through the coating. While such low frequencies are feasible experimentally, they are impractical because of the long image-formation times required for point-scanning techniques because the dwell time at each point in the image must be at least a few periods of the beam modulation frequency. These problems can be overcome by a parallel detection technique that monitors the temperature of a number of points on the specimen simultaneously. We have been pursuing such an approach, using an infrared scanner to image the surface temperature of the specimen as a function of time while a heating pulse is applied to the sample.

The instrumentation used in the time-resolved infrared technique is illustrated in Fig. 2. The heating source is an argon-ion laser with the beam gated by an acousto-optic modulator to allow heating pulses of various durations to be selected. The laser beam passes through a hole in an infrared reflector (beamsplitter) and illuminates the coated specimen. The infrared radiation from the specimen is then reflected at the beamsplitter and is detected by an infrared scanner.

The scanner has two modes of operation, *x-y* mode and time-trace mode (Fig. 3). In the *x-y* scan mode, the surface temperature, $T_s(x\text{-}y)$, is measured and the position of the center of the heating spot can be accurately located. In the time-trace mode, the vertical (y) scanning mirror is disabled, and the image displays $T_s(x,y_0)$ on the horizontal axis and time on the vertical axis. The surface temperature at the center of the heating spot can then be monitored as a function of time by selecting the appropriate vertical line scan from the time-trace image. If a background image is made before the heating pulse is turned on, the increase in surface temperature resulting from the application of the heating pulse can be determined as a function of time by subtracting the background image from the heating-pulse image. This procedure is shown in Fig. 4, which shows (a) an area scan image for an aluminide coating on a superalloy substrate, (b) the time-trace image with heating pulse, (c) the background time-trace image before the heating pulse, and (d) the heating pulse image minus the background image.

A one-dimensional model describing the evolution of the surface temperature during the time-resolved infrared experiment just described has been developed for a coating/substrate system.[11] This one-dimensional model indicates the role of parameters, such as coating thickness and thermal properties of the coating and substrate, on the temperature–time profiles. On the basis of this model, the temperature of the surface of a coating of thickness, l, after heating by a pulse of duration, τ, is given by

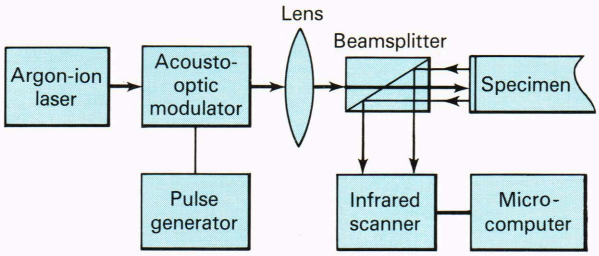

Figure 2—Instrumentation setup used in the time-resolved infrared technique.

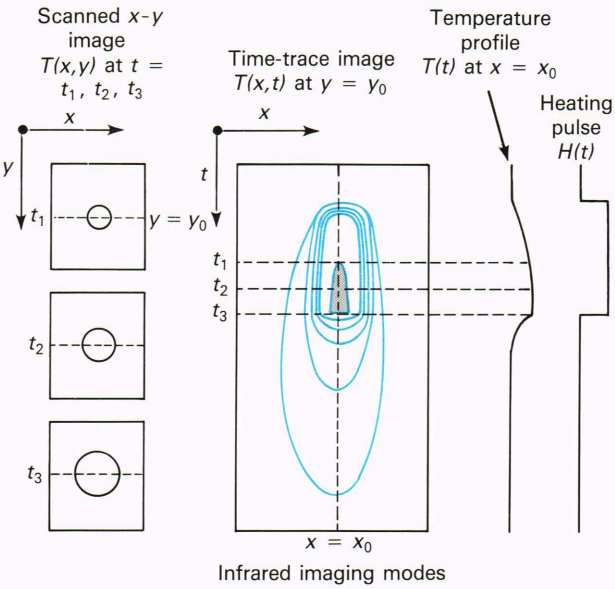

Figure 3—Comparison of area-scan (*x-y*) and time-trace (*x*-time) infrared imaging modes for measuring surface temperature $T(t)$ of a specimen illuminated by a heating pulse, $H(t)$.

$$T_{\text{total}}(t) = \begin{cases} T_1(t) + T_2(t) & \text{if } t < \tau \\ [T_1(t) - T_1(t-\tau)] + [T_2(t) - T_2(t-\tau)] & \text{if } t > \tau \end{cases} \quad (4)$$

where

$$T_1(t) = \left(\frac{1+\Gamma_0}{\sqrt{\pi k_c \rho_c C_c}}\right)\sqrt{t} \quad , \quad (5)$$

$$T_2(t) = \left(\frac{(1+\Gamma_0)(1+\Gamma_0^{-1})}{\sqrt{\pi k_c \rho_c C_c}}\right)\sum_{n=1}^{\infty}(\Gamma_0\Gamma)^n \times \left[\sqrt{t}\,\exp(a_n^2/t) + \sqrt{\pi}\,a_n[\text{erf}(a_n/t) - 1]\right], \quad (6)$$

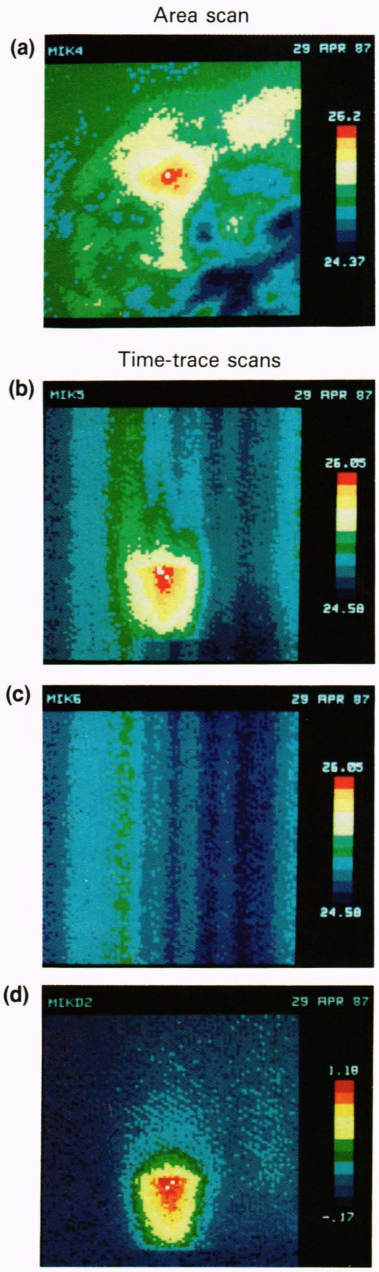

Figure 4—Examples of area-scan and time-trace images for an aluminide coating, showing the effect of background subtraction: (a) the area scan image for an aluminide coating on a superalloy substrate, (b) the time-trace image with the heating pulse, (c) the background time-trace image before the heating pulse, and (d) the heating-pulse image minus the background image.

and $a_n = nl/\sqrt{\alpha}$, (7)

where α is the thermal diffusivity. In these expressions Γ describes the thermal mismatch between the coating and the substrate, and Γ_0 describes the thermal mismatch between the coating and the gas. These factors are given by

$$\Gamma = (Y_g - Y_c)/(Y_g + Y_c)$$

$$\Gamma_0 = (Y_s - Y_c)/(Y_s + Y_c) , \quad (8)$$

where Y is the inverse thermal effusivity given by

$$Y = 1/(k\rho C)^{1/2} . \quad (9)$$

Throughout these expressions, the subscripts g, c, and s refer to the gas, coating, and substrate, respectively. The expression for the total surface temperatures (Eq. 4) may be thought of in terms of its constituent parts: T_1, the surface temperature obtained for the case of a semi-infinite medium, and T_2, the adjustment to the surface temperature resulting from the finite thickness of the coating and the presence of the substrate.

Figure 5a shows calculated values of T_1, T_2, and T_{total} for the case of an insulating coating on a conductive substrate exposed to a heating pulse of 1-s duration. As shown by Eq. 5, T_1 is dependent on the square root of time (root-time) while the heating pulse is applied, but decays after the heating pulse is turned off. When the substrate is more conducting than the coating (as in this example), T_2 is negative because heat readily flows into the substrate. The surface temperature of the coating is then pulled down below a root-time dependence after a characteristic time ($\approx$ 0.4 s in this example) that depends on the coating thickness and on the coating thermal properties.

The dependence of the surface temperature on coating thickness is illustrated in Fig. 5b, which gives the calculated temperature–time profiles for 0.2-, 0.4-, and 0.6-mm-thick ceramic coatings on a metal substrate for a heating pulse of 1-s duration. Included for comparison is the root-time behavior for a semi-infinite medium. As coating thickness decreases, the time at which the temperature–time profile deviates from the root-time behavior also decreases because of the shorter thermal transit time from the coating surface to the coating/substrate interface. A similar decrease in the characteristic time is observed as the thermal diffusivity of the coating is increased.

The role of thermal properties of the substrate in determining the temperature–time profile is illustrated in Fig. 5c, where an insulating substrate is compared with two conducting substrates having different conductivities. The semi-infinite root-time dependence is also shown in Fig. 5c for comparison. These curves show the variations in the temperature–time profiles that might be expected between regions of coating that are well bonded to a conductive substrate and regions that have become unbonded and may have a thermally insulating air layer between the coating and the substrate.

A number of time-resolved infrared experiments have been conducted on test specimens and engineering specimens of ceramic coatings on metal substrates, using the instrumentation system shown in Fig. 2. Figure 6 shows the effect of varying the thermal properties of the sub-

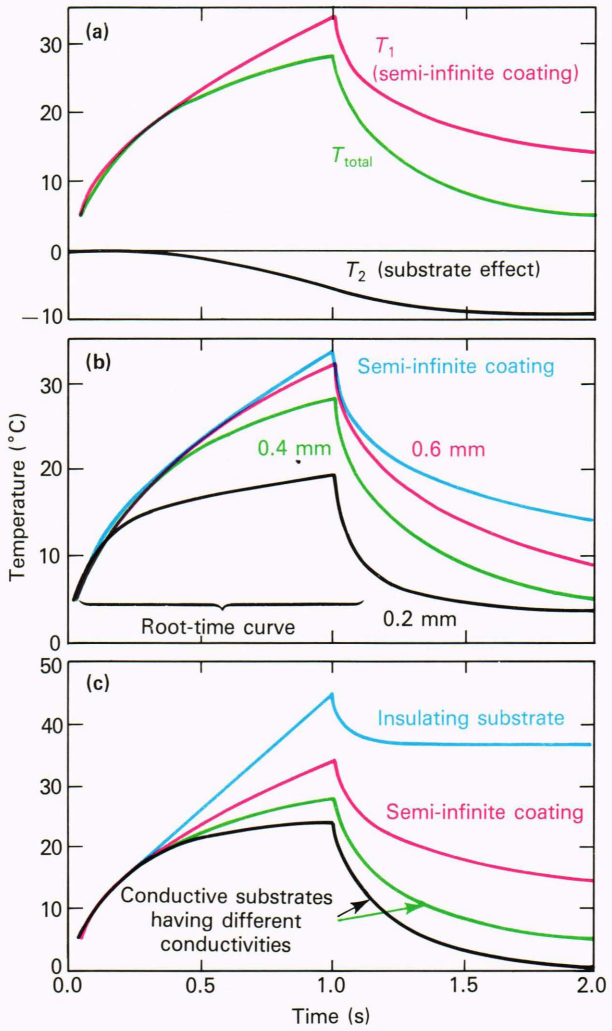

Figure 5—Theoretical plots showing: (a) the total surface temperature, T_{total}, and its component terms, T_1 and T_2; (b) the effect of coating thickness on the surface temperature of a layered specimen during heating by a square-wave heating pulse; (c) the effect of the thermal effusivity of the substrate on the surface temperature of a layered specimen.

strate for a 0.79-mm-thick glass specimen coated with platinum black with (a) an insulating air substrate and (b) a conductive aluminum substrate. These temperature data are plotted versus the square root of time to emphasize the early root-time dependence. After the characteristic time, which depends on the thickness and thermal diffusivity of the glass layer, the surface temperature decreases below the root-time behavior for the conducting substrate and increases above root-time for the insulating substrate, as is expected from Fig. 5c.

THERMOELASTIC TECHNIQUES

The specimen's thermoelastic response can also be used to monitor thermal properties and specimen structure. Sensor techniques include the use of piezoelectric transducers attached to the specimen and of noncontact optical methods such as laser interferometry. With these detection methods, a "thermal" nondestructive evaluation technique takes on some of the characteristics of ultrasonic nondestructive evaluation methods. In fact, since the development of laser generation and interferometric detection of ultrasound,[12] the similarities between the techniques become more pronounced: In ultrasonics, the specimen's transient response to pulsed excitation from a laser (or other source) is monitored as a function of time. Images are constructed by following the amplitude of a particular feature in the displacement-time waveform as a function of position over the sample. In thermal-wave imaging using thermoelastic detection, the excitation is typically a continuous-wave-modulated pump beam, and, to construct images, the magnitude and phase of the transducer response are monitored as a function of position over the specimen. The modulation frequency of the beam can then be changed to vary the thermal-diffusion length in the specimen.

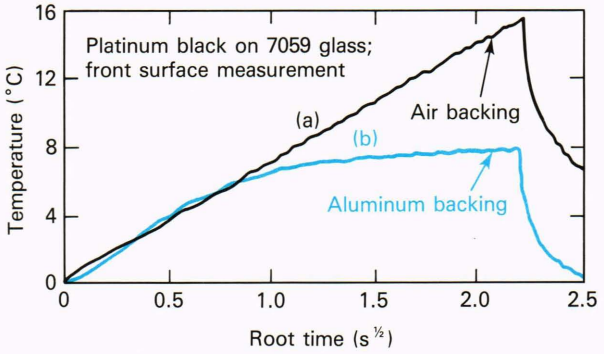

Figure 6—Surface temperature versus time for a glass layer coated with platinum black (a) on an air substrate and (b) on an aluminum substrate.

There is a strong thermal contribution to the thermoelastic image. The ratio of the thermal wavelength to the acoustic wavelength is $(\alpha f)^{1/2}/V$, where α is the thermal diffusivity, f is the frequency, and V is the velocity of the elastic disturbance. The thermal wavelength is then typically a thousand times smaller than the acoustic wavelength. Hence images having much higher spatial resolution can be obtained by thermoelastic imaging than is possible by conventional ultrasonic imaging techniques for similar frequency ranges (100 kHz to 10 MHz). Comparably high resolutions can be obtained by advanced ultrasonic techniques such as scanning acoustic microscopy, but those techniques require modulation frequencies in the gigahertz range.

Experimentally, implementation of the thermoelastic technique with a piezoelectric sensor is quite simple, and measurements can be made even inside the vacuum chamber of a scanning electron microscope or a secondary-ion mass spectrometer. This method allows the electron-beam/specimen (or ion-beam/specimen) interactions to be studied in their role of forming thermal-wave images.[13] Further investigations have focused on the effect of light and oxygen on the ion/acoustic generation process in semiconductors.[14] The role of the elastic parameters of the specimen in determining the contrast seen in thermoelastic images was studied by comparing thermal and thermoelastic images of the same

specimen. It was found that variations in the elastic parameters of the material can be imaged directly by using thermoelastic thermal-wave imaging.[15] For layered structures, an important experimental finding has been that thermoelastic techniques can detect defects at depths greater than the thermal diffusion length and hence greater than can be sensed by purely thermal detection techniques.[16]

An example of thermoelastic imaging of a protective coating on a superalloy substrate is shown in Fig. 7. This image shows contrast in areas adjacent to regions where local spalling of the coating had occurred. Variations in signal magnitude and phase may indicate decohesion of the coating from the substrate in these areas. This decohesion could not be sensed easily by the continuous-wave-modulated thermal-wave technique because the coating was much thicker than the thermal diffusion length for the modulation frequencies normally used.

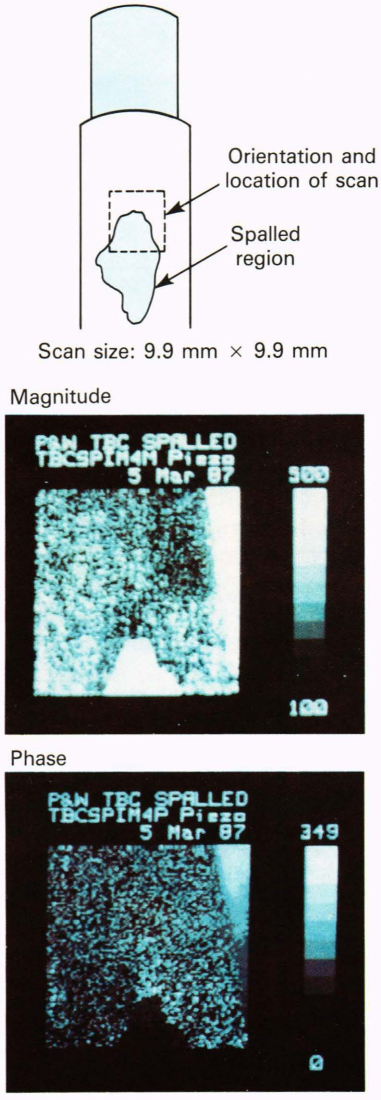

Figure 7—Thermoelastic image of ceramic-barrier coating in the region of a spalled coating.

INTERNAL PROBING BY OPTICAL BEAM DEFLECTION

In one of the conventional thermal-wave imaging detection techniques shown in Fig. 1, an optical beam interrogates the temperature distribution in the air layer above a periodically heated specimen. The probe beam passes above the sample and is deflected by the gradient in the refractive index of the air, produced by heat flow from the specimen. Two deflection components of the probe beam are monitored. The normal component is in the plane defined by the probe beam and the specimen-surface normal, which is dependent on the surface temperature of the specimen. The transverse component is the deflection in the plane parallel to the specimen surface and is dependent on the gradient of the temperature distribution orthogonal to the path of the probe beam. Cross-sectional images of the magnitude and phase of these two components are shown in Fig. 8. Here, the pump beam is incident from the top of the image onto an insulating glass substrate, and, because of the low thermal diffusivity of glass, a very localized temperature distribution is produced in the specimen. The thermal lens in the air is then imaged by scanning the probe beam through a series of x positions on either side of the position of the pump beam on the specimen and for a series of y positions representing different heights of the probe beam above the specimen surface. The result is an image of the dependence of the deflection signal on pump/probe offset (x) and probe/specimen offset (y). Note that while the magnitude image of the normal component is greatest for a pump/probe offset of zero, that of the transverse component is minimum at this position and the phase image shows a 180° phase excursion because the temperature gradient here is zero. The magnitude image of the normal component also shows two lobes adjacent to the central maximum. The lobes are predicted theoretically[17] and occur when the thermal diffusion length in air is greater than the spatial extent of the temperature distribution on the specimen surface.

If the material under investigation is transparent at the probe-beam wavelength, it is possible to develop a variation of the conventional optical-beam-deflection method by probing the temperature distribution inside the material directly. This procedure is in contrast to the indirect measurement of specimen temperature, obtained by probing the thermal lens in the air layer above the specimen. Internal optical-beam-deflection measurements make possible direct measurement of material absorption coefficients for optical, X-ray, and microwave sources. When a specimen is heated by electromagnetic radiation of some given wavelength, the heat deposited per unit distance into the material depends on the absorption coefficient at that wavelength. Since the internal optical-beam-deflection technique allows the temperature distribution in the specimen to be mapped as a function of distance into the material, values for the absorption coefficient can be obtained directly.

Figure 9 shows the results of a calculation of the thermal flux as a function of position on either side of an

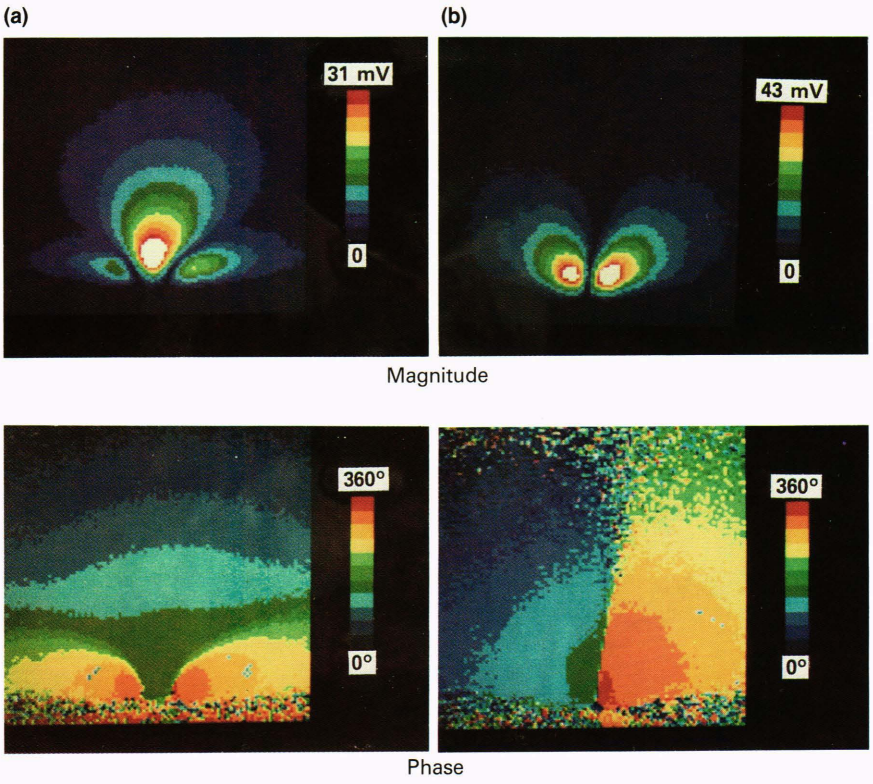

Figure 8—Optical-beam-deflection images showing the cross section of the thermal lens in air over a thermally insulating glass substrate for both the (a) normal and (b) transverse components of the deflection.

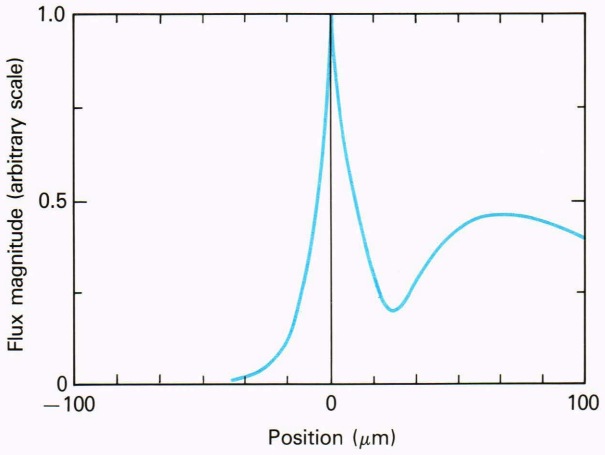

Figure 9—Thermal flux versus position on either side of the interface between a transparent coating and a substrate with $\beta = 50$.

interface between a transparent coating and a substrate with $\beta = 50$.[3] Since the coating layer (values of position less than zero) is transparent, the heat from the pump beam is deposited directly at the interface. The thermal flux within the coating then depends only on the thermal parameters of the coating. In the substrate, the thermal flux changes rapidly with distance from the interface, depending on the relative magnitudes of the optical absorption length and the thermal diffusion length. Initial experiments, conducted in collaboration with W. Sachse of Cornell University, using the Cornell High-Energy Synchrotron Source, have involved studies of X-ray absorption coefficients in a number of materials. Theoretical work is under way to allow the absorption coefficients to be obtained for the three-dimensional case of a probe beam of finite extent.

The optical-beam-deflection technique, using a subbandgap probe beam, can also be used to characterize the thermal and electrical transport properties of semiconductors.[18,19] Our experiments have focused on the characterization of cadmium sulfide, a semiconductor that is sufficiently transparent to allow a helium–neon probe beam to pass through the crystal. These studies will soon be extended to other semiconductors with the implementation of an optical-beam-deflection system at infrared wavelengths.

There are three different contributions to the refractive index gradient inside a semiconductor illuminated by light: (1) a temperature gradient produced by diffusion of heat from the heated surface of the specimen; the extent of this gradient depends on the thermal diffusivity of the material; (2) a modification of the temperature gradient by the transport and recombination of photocarriers over a distance from the surface, determined by electron diffusion; and (3) a concentration gradient of free carriers that contributes to the index gradient directly. Summing these three components of the index gradient produces a cusp in plots of the deflection signal as a function of either modulation frequency or distance from the specimen surface.

Figure 10 shows the frequency dependence of the temperature gradient in silicon for five different distances

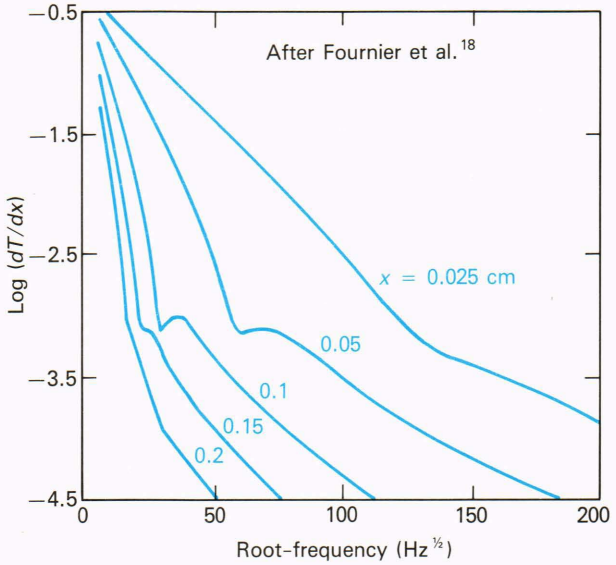

Figure 10—Theoretical plots showing the frequency dependence of the temperature gradient in silicon, resulting from both thermal diffusion and carrier recombination.

into a silicon specimen. The curves were calculated using the theoretical model presented in Ref. 18. The shapes of the curves reflect the effect of the various contributions to the index gradient and allows values for the thermal and electronic properties to be obtained from measurements of the deflection signal as a function of modulation frequency and position from the specimen surface.

Experimental results for the frequency dependence of the deflection signal in cadmium sulfide are shown in Fig. 11. Also shown, for comparison, is the deflection signal as a function of frequency in the air layer just above the specimen. The cadmium sulfide curve has a distinct cusp that separates the "thermal regime" at low frequencies from the "electronic regime" at higher frequencies. The slope of the curve in the thermal regime allows the thermal diffusivity in cadmium sulfide to be calculated and is in agreement with published values.

Further internal optical-beam-deflection experiments involved constructing images of the deflection as shown in Fig. 12 by raster-scanning the probe beam horizontally across the pump beam and vertically above and below the sample surface. This scan geometry is analogous to that used to construct the images of the thermal lens shown in Fig. 8. The image on the left was obtained using a modulation frequency of 10 Hz; the vertical scale indicates the thermal-diffusion length in cadmium sulfide at this frequency. While there are nonuniformities in the signal intensity at different positions in the specimen, the overall effect does not extend much deeper than the thermal-diffusion length, as would be found in a specimen exhibiting simple thermal diffusion of heat applied at the surface. The image on the right was obtained using 600 Hz; again, the thermal-diffusion length is indicated by the vertical scale. In this image, however, the signal extends deeper than a thermal-diffusion length into the specimen, indicating the role of electronic diffusion

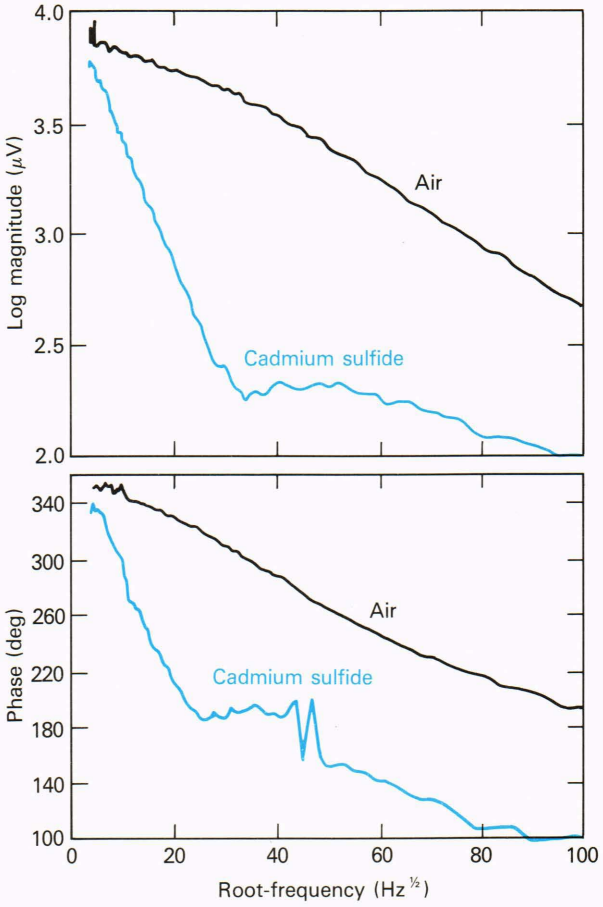

Figure 11—Frequency dependence of the internal optical-beam-deflection signal in cadmium sulfide for laser excitation.

and subsequent recombination of the carriers on the temperature gradient in the specimen. The spatial variations in the optical-beam-deflection signal seen in both images indicate variations in both thermal and electronic effects, possibly related to structure variations in the semiconductor.

We have recently extended the internal optical-beam-deflection measurements by using an electron beam to excite the semiconductor inside a scanning electron microscope. The instrumentation system used is illustrated in Fig. 13. Both thermal and electronic components to the index gradient are observed in the frequency dependence of the deflection, as seen in Fig. 14. It is hoped that this technique will make it possible to determine the distribution of primary electrons by direct experimental measurement. The internal optical-beam-deflection technique may further provide the ability to examine electron/specimen interaction ranges in semiconductors, a subject that is important to the implementation of electron lithography techniques for microelectronics fabrication. Extension of these techniques to imaging should allow local parameter variations to be determined and could have application in deep trap characterization in semicondictors where the trap may act as a scattering or recombination site.

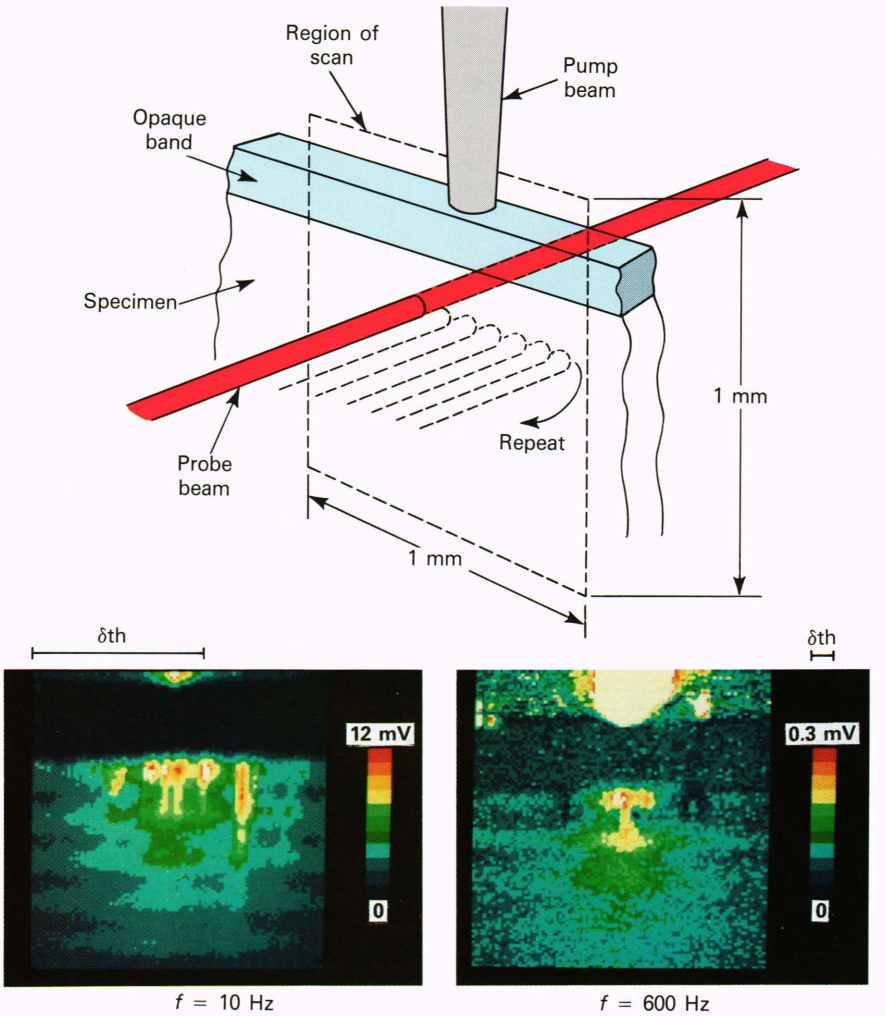

Figure 12—Internal optical-beam-deflection images in cadmium sulfide for two modulation frequencies (10 and 600 Hz).

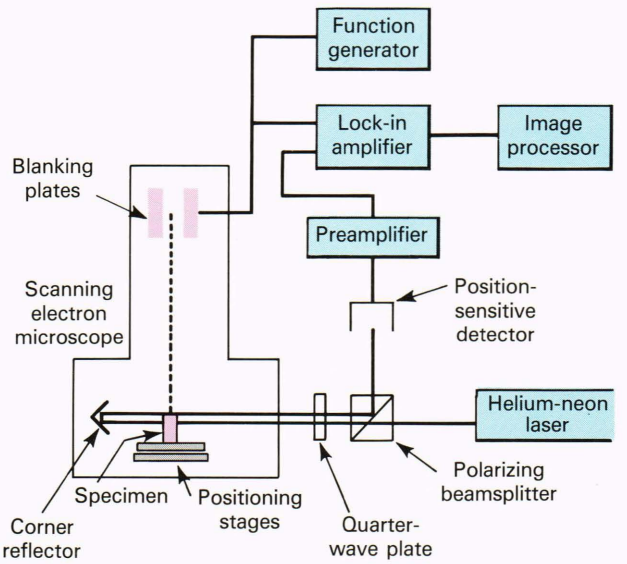

Figure 13—Instrumentation setup for electron/optical-beam-deflection experiments inside the scanning electron microscope.

CONCLUSIONS

Many types of new composite materials for a wide range of important technological applications are currently used in all kinds of structures, ranging from fighter aircraft to microelectronic circuits. Many of these materials systems rely heavily on the properties of interfaces and layered structures to provide the improved characteristics needed for the applications. Three types of thermal nondestructive techniques for evaluating layered structures and interfaces have been discussed in detail. Time-resolved infrared techniques show promise for use with large specimens because these techniques make it possible to monitor areas of large structures directly by providing nearly parallel processing of surface-temperature information, making it possible for these methods to acquire thermal-wave images much faster than the scanning methods and providing a way to deal with thick specimens having low thermal diffusivity. Thermoelastic detection techniques, although complicated to describe theoretically, provide a number of specific advantages not found with other techniques, specifically the ability to detect defects at greater depths than the purely ther-

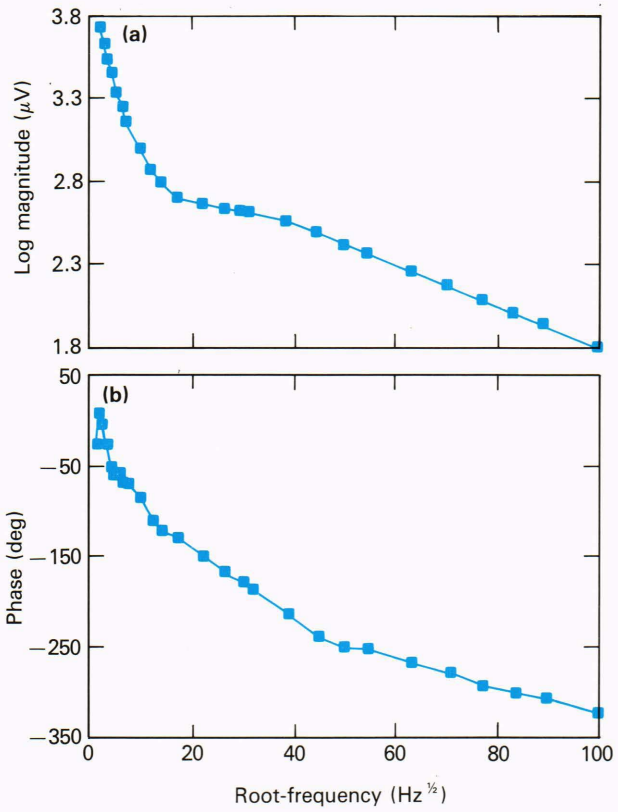

Figure 14—Frequency dependence of the electron/optical-beam-deflection signal in cadmium sulfide: (a) magnitude versus the square root of frequency, (b) phase versus the square root of frequency.

mal methods and the sensitivity to variations in elastic properties. Finally, the internal optical-beam-deflection techniques provide new methods for measuring a number of material properties, including absorption coefficients, thermal and electronic diffusivities, minority carrier lifetimes, and recombination times.

REFERENCES

[1] J. C. Murphy, J. W. Maclachlan, and L. C. Aamodt, "Image Contrast Processes in Thermal and Thermoacoustic Imaging," *IEEE Trans. Ultrason. Ferroelectr. Freq. Control* **UFFC-33**, 529–541 (1986).

[2] J. C. Murphy, L. C. Aamodt, F. G. Satkiewicz, R. B. Givens, and P. R. Zarriello, "Materials and Microstructure," *Johns Hopkins APL Tech. Dig.* **7**, 187–199 (1986).

[3] J. C. Murphy, J. W. Maclachlan, and L. C. Aamodt, "The Role of Thermal Wave Techniques in Materials Characterization," in *International Advances in NDT*, W. J. McGonnagle, ed., Gordon and Breach, New York (1988).

[4] D. P. Almond, P. M. Patel, I. M. Pickup, and H. Reiter, "An Evaluation of the Suitability of Thermal Wave Interferometry for the Testing of Plasma Sprayed Coatings," *NDT International* **18**, 17–24 (1985).

[5] D. L. Balageas, J. C. Krapez, and P. Cielo, "Pulsed Photothermal Modeling of Layered Materials," *J. Appl. Phys.* **59**, 348–357 (1986).

[6] J. C. Murphy, J. W. Maclachlan, and L. C. Aamodt, "Thermal Imaging of Barrier Coatings on Refractory Substrates," in *Review of Progress in Quantitative Nondestructive Evaluation*, D. O. Thompson and D. E. Chimenti, eds., Vol. 7, Plenum Press, New York, pp. 245–252 (1988).

[7] A. C. Tam and B. Sullivan, "Remote Sensing Applications of Pulsed Photothermal Radiometry," *Appl. Phys. Lett.* **43**, 333–335 (1983).

[8] N. Tsutsumi and T. Kiyotsukuri, "Measurement of Thermal Diffusivity for Polymer Film by Flash Radiometry," *Appl. Phys. Lett.* **52**, 442–444 (1988).

[9] F. H. Long, R. R. Anderson, and T. F. Deutsch, "Pulsed Photothermal Radiometry for Depth Profiling of Layered Media," *Appl. Phys. Lett.* **51**, 2076–2078 (1987).

[10] W. P. Leung and A. C. Tam, "Noncontact Measurement of Thermal Conductivity of Epoxy Bonds by Pulsed Photothermal Radiometry," *Appl. Phys. Lett.* **51**, 2085–2087 (1987).

[11] J. W. Maclachlan, L. C. Aamodt, and J. C. Murphy, "Characterization of Ceramic Coatings by Advanced Nondestructive Evaluation Methods," in *Proc. 12th Annual Conf. on Composites and Advanced Ceramic* (to be published, 1988).

[12] D. A. Hutchins, "Pulsed Photoacoustic Materials Characterization," *IEEE Trans. Ultrason. Ferroelectr. Freq. Control* **UFFC-33**, 429–449 (1986).

[13] J. C. Murphy, L. C. Aamodt, J. W. Maclachlan, and F. G. Satkiewicz, "Ion-Acoustic Imaging of Subsurface Flaws in Aluminum," in *Review of Progress in Quantitative Nondestructive Evaluation*, D. O. Thompson and D. E. Chimenti, eds., Vol. 5A, Plenum Press, New York, pp. 455–463 (1986).

[14] F. G. Satkiewicz, J. C. Murphy, and L. C. Aamodt, "Light Enhanced Ion-Acoustic Signal Generation in Si and GaAs," in *Photoacoustic and Photothermal Phenomena*, P. Hess and J. Pelzl, eds., Springer Series in Optical Sciences, Springer-Verlag, Berlin, Heidelberg, pp. 288–291 (1988).

[15] J. W. Maclachlan and J. C.Murphy, "Anisotropy in Thermoacoustic Imaging of Single Crystals," in *Photoacoustic and Photothermal Phenomena*, P. Hess and J. Pelzl, eds., Springer Series in Optical Sciences, Springer-Verlag, Berlin, Heidelberg, pp. 294–297 (1988).

[16] J. C. Murphy, J. W. Maclachlan, R. B. Givens, F. G. Satkiewicz, and L. C. Aamodt, "The Generation of Ultrasound by Laser, Electron and Ion Probes and Its Application to the Characterization of Materials," in *Proc. Ultrasonics International 1985*, Butterworths Scientific, London, pp. 30–36 (1985).

[17] L. C. Aamodt, J. C. Murphy, and J. W. Maclachlan, "Image Distortion in Optical Beam Deflection Imaging," in *Photoacoustic and Photothermal Phenomena*, P. Hess and J. Pelzl, eds., Springer Series in Optical Sciences, Springer-Verlag, Berlin, Heidelberg, pp. 385–388 (1988).

[18] D. Fournier, A. C. Boccara, A. Skumanic, and N. M. Amer, "Photothermal Investigation of Transport in Semiconductors: Theory and Experiment," *J. Appl. Phys.* **59**, 787–795 (1986).

[19] J. W. Maclachlan, J. C. Murphy, and L. C. Aamodt, "Sub-Bandgap Probing for Characterization of CdS," *Bull. Am. Phys. Soc.* **33**, 301 (1988).

ACKNOWLEDGMENTS—Funding for this work was provided by the Department of the Navy under contract N00039-87-C-5301 and by the Center for Nondestructive Evaluation, The Johns Hopkins University, Baltimore.

THE AUTHORS

JOHN C. MURPHY is a physicist in the Materials Science Group in the Milton S. Eisenhower Research Center. Born in Wilmington, Del., he obtained a B.A. degree from The Catholic University of America in 1957, an M.S. from Notre Dame University in 1959, and a Ph.D. from The Catholic University in 1970. His work at APL has included experimental studies of excitation transfer in luminescent systems using optical and microwave spectroscopy, measurement of nonradiative relaxation processes using photoacoustic spectroscopy, and, more recently, thermal wave imaging as well as remote sensing of corrosion using AC magnetometry. He is currently a research professor in the Materials Science and Engineering Department of The Johns Hopkins University and a member of the Executive Committee of the Johns Hopkins Center for Nondestructive Evaluation, a corporately funded interdisciplinary center involving participation of the Homewood and Medical School faculties and APL's Research Center.

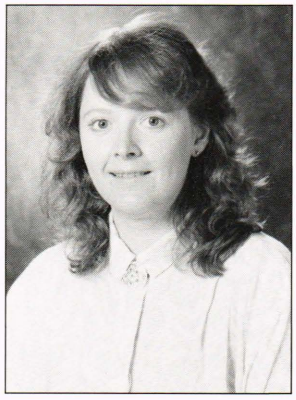

JANE W. MACLACHLAN is a materials scientist in the Materials Science Group of APL's Milton S. Eisenhower Research Center. She was born in Glasgow, Scotland, and earned a B.S. degree in physics in 1979 and an M.S. degree in metallurgical engineering in 1983 from Queen's University, Kingston, Ontario, Canada. During 1979–83, she worked as a research officer in the Physics Department of the Royal Military College, Kingston, investigating the acoustic emission behavior of aluminum alloys during fatigue crack growth and the application of acoustic emission as a nondestructive evaluation technique for in-flight monitoring of aircraft components. She then obtained a Ph.D. in materials science and engineering from The Johns Hopkins University and joined APL in 1986. Her recent research interests include the development and application of photothermal and thermoacoustic measurement techniques for nondestructive evaluation and materials characterization.

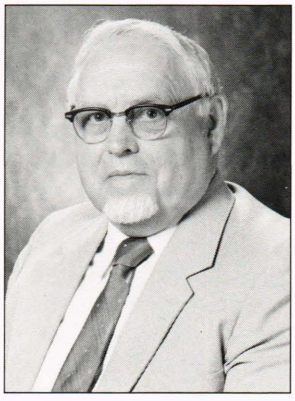

LEONARD C. AAMODT is a physicist in the Materials Science Group of APL's Milton S. Eisenhower Research Center. He was born in Salt Lake City and earned a B.S. degree in electrical engineering from the University of Utah in 1943 and a Ph.D. from Columbia University in 1955. During World War II, he worked at the Westinghouse Research Division and on the Manhattan District Project in Brooklyn, in Oak Ridge, and at Columbia University. Before joining APL, he was an assistant professor in the Departments of Mathematics, Physics, and Electrical Engineering at Brigham Young University in Provo, Utah. His work at APL has included a study of excitation transfer in luminescent systems, nonradiative relaxation processes, and photoacoustic spectroscopy. His current work includes photothermal imaging, and characterization and nondestructive evaluation of materials.